ACS APPLIED MATERIALS & INTERFACES

Research Article

www.acsami.org

Role of Surface Functional Groups in Ordered Mesoporous Carbide-Derived Carbon/Ionic Liquid Electrolyte Double-Layer Capacitor Interfaces

Katja Pinkert,*[,†,‡] Martin Oschatz,[§] Lars Borchardt,[§] Markus Klose,[†] Martin Zier,[†] Winfried Nickel,[§] Lars Giebeler,[†,‡] Steffen Oswald,[†] Stefan Kaskel,[§] and Jürgen Eckert[†,‡]

[†]Leibniz-Institute for Solid State and Materials Research (IFW) Dresden e.V., Institute for Complex Materials, P.O. Box 270116, D-01171 Dresden, Germany

[‡]Institut für Werkstoffwissenschaft, Technische Universität Dresden, Helmholtzstraße 7, D-01069 Dresden, Germany

[§]Anorganische Chemie, Technische Universität Dresden, Bergstraße 66, D-01069 Dresden, Germany

ABSTRACT: Ordered mesoporous carbide-derived carbon (OM-CDC) with a specific surface area as high as 2900 m^2 g^{-1} was used as a model system in a supercapacitor setup based on an ionic liquid (IL; 1-ethyl-3-methylimidazolium tetrafluoroborate) electrolyte. Our study systematically investigates the effect of surface functional groups on IL-based carbon supercapacitors. Oxygen and chlorine functionalization was achieved by air oxidation and chlorine treatment, respectively, to introduce well-defined levels of polarity. The latter was analyzed by means of water physisorption isotherms at 298 K, and the functionalization level was quantified with X-ray photoelectron spectroscopy. While oxygen functionalization leads to a decreased capacitance at higher power densities, surface chlorination significantly improves the rate capability. A high specific capacitance of up to 203 F g^{-1} was observed for a chlorinated OM-CDC sample with a drastically increased rate capability in a voltage range of ±3.4 V.

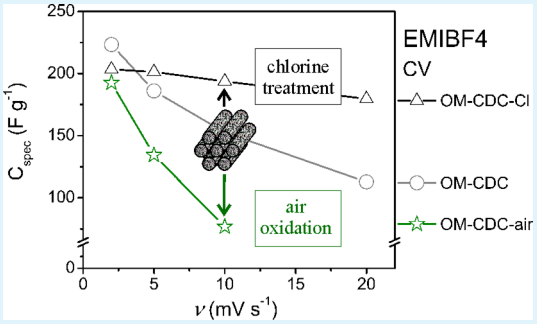

KEYWORDS: *supercapacitor, ordered mesoporous carbide-derived carbons, halogenation surface treatment, ionic liquid electrolyte*

1. INTRODUCTION

The increasing demand for powered mobile devices quickly advances the field of energy storage. Rechargeable batteries based on the lithium-ion intercalation mechanism, conversion-type electrodes, and lithium−air- and lithium−sulfur-based energy storage concepts are widely investigated to power the 21st century.[1−5] These most prominent and latest battery-type devices exemplify the great variety of faradaic redox systems for electrical power storage. Despite their high energy density compared to classic rechargeable devices such as lead-acid batteries, lithium-ion batteries still suffer from low power densities and limited cycle life especially compared to supercapacitors. The main reason for overcoming these limitations is the purely physical charge storage mechanism of supercapacitors based on electrostatic interactions of electrolyte ions on charged electrode surfaces.[1,4,6−9] The electrostatic charge storage within the formed interface layer is very fast compared to faradaic redox reactions of bulk battery electrodes, with the latter being often limited by ion diffusion processes. Furthermore, the electrostatic charge storage at the formed interface is highly reversible and therefore displays long cycle stability.[10,11] Commercial supercapacitors consist of two symmetrical activated carbon electrodes. Electrolytes based on quaternary ammonium salts dissolved in acetonitrile provide high ionic conductivities for high power application (up to 10 kW kg^{-1}) and an operative voltage range of up to 2.7 V, significantly enhancing their energy density compared to aqueous electrolytes.[10−12] However, the energy density of already commercialized electrical double-layer capacitors (EDLCs) is still at least 1 order of magnitude lower compared to secondary batteries and therefore limits their application to recuperation devices or peak power buffering.[1,11]

To widen the application range of supercapacitors by increasing the specific energy density, optimization strategies for both electrode materials and electrolytes are reported in the literature. As one strategy, the electrode material is designed toward defined pore structures, narrow pore-size distributions (PSDs), and ultrahigh specific surface areas (SSAs).[13,14] These characteristics can help to improve the specific capacitance of the electrode material. Hexagonally ordered mesoporous carbide-derived carbons (OM-CDCs) are well-known for the presence of a hierarchical micro- and mesopore system with high nanopore volumes (causing slightly lower volumetric capacitances compared to purely microporous materials because of the lower material density), well-defined pore sizes, as well as high SSAs and therefore excellent gravimetric

Received: December 2, 2013
Accepted: January 23, 2014
Published: January 23, 2014

capacitive performance exceeding 200 F g^{-1} in supercapacitors.[13−16] As an alternative to the classic supercapacitor electrolytes, ionic liquids (ILs) are examined that provide up to 2 times higher operating voltage compared to the standard nonaqueous electrolyte systems, thus tremendously improving the overall energy density.[6,11,17−19] Among a large variety of IL electrolytes, 1-ethyl-3-methylimidazolium tetrafluoroborate ($EMIBF_4$) is proven to fit both high energy density and acceptable rate capability of supercapacitor devices even at room temperature.[6,11,13,20]

Because charge storage of the EDLC takes place at the interface of the electrode material and the electrolyte within the porous network of the electrode, the pore size, the pore geometry, and, even more importantly, the interaction of the surface of the electrode material with the electrolyte are the characteristics influencing the EDLC performance.[6,12,21−23] Compared to classic electrolytes, ILs are characterized by higher viscosities and changed wetting behavior on porous electrodes.[7,11,21] To guarantee the rate capability and cycling stability at a high level while switching the electrolyte system, the mentioned characteristics of the porous carbon compound become even more important to be tailored for each IL electrolyte. While some groups investigate the influence of micropore size effects on the maximum specific capacitance of carbon materials in combination with IL electrolytes,[20,22,24,25] others accentuate the need for mesopores to allow rapid ion diffusion for effective charging and discharging.[12,18,21,26,27] Although the importance of a tailored surface functionality of carbon electrodes was recently outlined,[12,18,21] detailed analytical insight into surface defects and their influence on the supercapacitor performance using IL electrolytes is rare.

We herein report a systematic study about the influence of surface functionalization on the capacitance performance of hierarchical micro- and mesoporous carbide-derived carbons. The materials are used as supercapacitor electrodes in combination with $EMIBF_4$ IL as the electrolyte, a hydrophilic IL miscible with water.[28]

2. MATERIALS AND METHODS

2.1. Synthesis of Hexagonally OM-CDC. The pristine OM-CDC sample was prepared by mixing 2.0 g of ordered mesoporous SiO_2 (SBA-15 hydrothermally treated at 403 K) with a mixture of 2.1 mL of liquid allylhydridopolycarbosilane (SMP-10, Starfire) and 0.5 mL of the cross-linker *p*-divinylbenzene by the incipient wetness method. Pyrolysis of the resulting SMP-10/SBA-15 composite under flowing argon was performed at 1073 K for 2 h at a heating rate of 60 K h^{-1}. Silica dissolution was achieved by treating the composite material in a hydrofluoric acid (35% aqueous solution)/water/ethanol mixture (1:1:1 by volume) for 3 h followed by washing with ethanol. Then, 1.0 g of the mesoporous carbide was transferred into a quartz boat and placed in a horizontal tubular furnace equipped with a quartz tube. After it was flushed with 150 mL min^{-1} of argon, the material was heated to 1073 K at a rate of 450 K h^{-1}. When that value was reached, the gas flow was changed to a mixture of 80 mL min^{-1} of chlorine and 70 mL min^{-1} of argon. After 3 h of chlorine treatment, the furnace was cooled to 873 K under an argon flow of 150 mL min^{-1}. At that temperature, the gas flow was changed to 80 mL min^{-1} of hydrogen for 1 h to remove chlorine and silicon chloride species adsorbed in the OM-CDC pores followed by natural cooling to room temperature under flowing argon.

2.2. Surface Functionalization of Pristine OM-CDC in Air (OM-CDC-Air). A total of 200 mg of the as-made OM-CDC was placed in a porcelain boat and transferred to a muffle furnace. The material was heated in air to a maximum temperature of 693 K for 1 h.

2.3. Surface Chlorination of Pristine OM-CDC (OM-CDC-Cl). A total of 200 mg of the as-made OM-CDC was placed in a quartz glass boat and placed in the isothermal zone of a tubular IR furnace (IRF 10, Behr). After it was flushed with 150 mL min^{-1} of argon, the material was heated to 1073 K within 5 min. Then, a mixture of 80 mL min^{-1} of chlorine and 70 mL min^{-1} of argon was applied for the duration of 30 min. Subsequently, the gas flow was changed to 150 mL min^{-1} of argon, and the material was allowed to cool to room temperature.

2.4. Characterization of Carbon Samples. Nitrogen physisorption experiments were carried out at 77 K using a Quantachrome Quadrasorb SI apparatus. Prior to measurement, the samples were degassed under a dynamic vacuum at 393 K for 12 h. The SSA was calculated using the multipoint Brunauer−Emmett−Teller (BET) method for p/p_0 = 0.05−0.2. The PSDs were obtained by employing the quenched solid density functional theory (QSDFT) adsorption model implemented in the Quantachrome *Quadrawin 5.05* software assuming a slit/cylindrical pore geometry for pristine and surface-modified OM-CDC samples. Water-vapor adsorption was performed at 298 K using a Quantachrome Hydrosorb apparatus. Raman spectra were recorded with an excitation laser wavelength of 532 nm using a Thermo Scientific DXR Smart Raman spectrometer [laser power of 9 mW, aperture of 50 μm (slit), resolution of 5.5−8.3 cm^{-1}, and spot size of 2.1 μm]. X-ray photoelectron spectroscopy (XPS) measurements were carried out on a PHI 5600 CI system (Physical Electronics) using monochromatized Al Kα_1 X-rays for excitation. The analyzer pass energy was 29 eV, and the binding energy scale of the spectrometer was calibrated using Au $4f_{7/2}$ (84.0 eV) and Cu $2p_{3/2}$ (932.7 eV). Partially, a low-energy electron beam was used for charge neutralization, and residual binding energy shifts were corrected using sample states where charging occurred. The atomic concentration quantification was performed using standard single-element sensitivity factors[29] assuming a homogeneous mixture of the elements in the analysis volume of some nanometer thickness. Thus, different surface states can be detected and qualitatively compared.

2.5. Electrochemical Characterization. The electrodes used for the symmetric two-electrode supercapacitor arrangement were prepared by mixing the porous carbon samples with a poly(vinylidene difluoride) (PVDF) solution in acetone. The resulting slurry consisted of a 95 wt % electroactive material and 5 wt % PVDF. To test the behavior of the pure electrode material, no extra conducting agent was added and no conductive paint or etching was applied to the aluminum current collector. The slurry was drop-coated onto a coin-shaped aluminum current collector with a diameter of 12 mm and dried at 353 K for 12 h. To avoid any contamination of the samples with surface moieties and physisorbed gaseous species, the electrodes were additionally activated for 12 h at 373 K in a vacuum. The vacuum oven was placed in an argon-filled glovebox (O_2 < 0.1 ppm; H_2O < 0.1 ppm). Each electrode contained about 4 mg of an electroactive material. The facing electrodes were electrically separated by a glass microfiber filter (Whatman GF/D, 1.2 mm) soaked with 200 μL of the IL electrolyte and placed in a Swagelok-type test cell. Electrochemical measurements were carried out at 298 K within a climate chamber using a multichannel potentiostat−galvanostat (VMP3, Bio-Logic, France). Prior to capacitance determination, based on the mass of active material of a single electrode for the symmetric two-electrode arrangement, 10 charge/discharge cycles were performed at a potential scan rate of 10 mV s^{-1}. To determine the capacitance at each scan rate, five charge/discharge cycles were measured. The fifth cycle is shown and considered for calculations. Capacitance values of the active material of a single electrode were determined from cyclic voltammetry (CV) experiments by eq 1,

$$C_{spec} = \frac{1}{\nu(V_2 - V_1)} \int_{V_1}^{V_2} I_{spec}\, dV \quad (1)$$

where C_{spec} is the specific capacitance (F g^{-1}) based on the mass of the electroactive material, ν is the potential scan rate (mV s^{-1}), and I_{spec} is the specific response current density (A g^{-1}) integrated over the

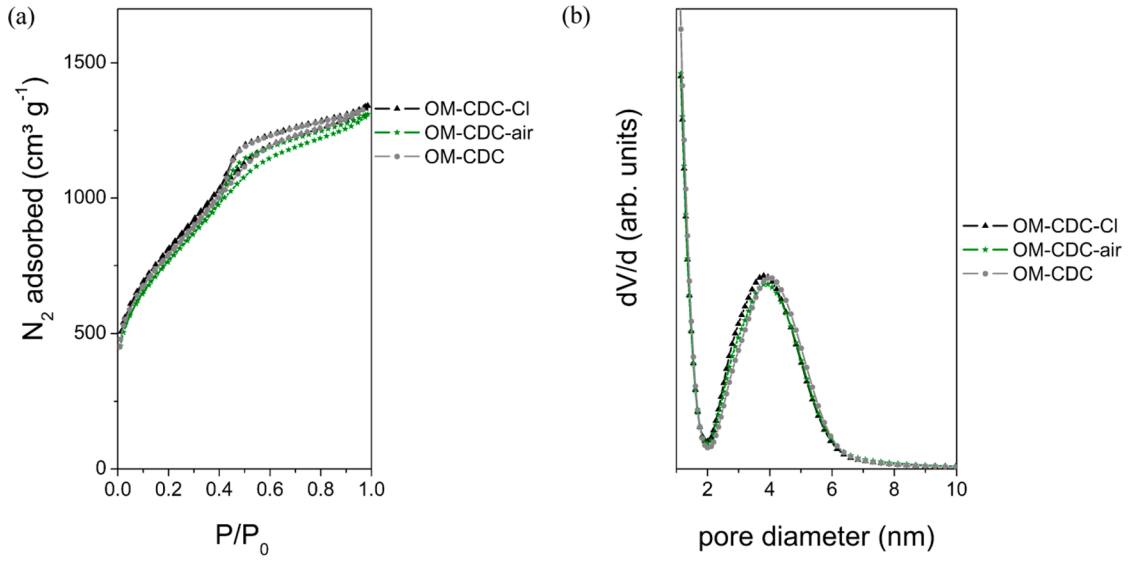

Figure 1. Porosity of the OM-CDC samples: (a) Nitrogen physisorption isotherms recorded at 77 K. (b) QSDFT PSD with a mixed kernel of cylindrical and slit pores applied.

applied potential window ($V_2 - V_1$), based on the mass of the electroactive material.

3. RESULTS AND DISCUSSION

The EDLC performance of porous carbons is mainly determined by the SSA accessible for the electrostatic charge storage due to adsorption of electrolyte ions. Here, IL electrolytes consisting of weakly coordinated organic ions with ion sizes in the range of 1 nm are discussed. The most important characteristics of carbon materials affecting the formation of the interface layer to perform the electrostatic charge storage are the pore size, pore geometry, and surface interaction of the electrode material with the electrolyte. Therefore, the OM-CDC model system was applied, characterized by a hexagonally ordered mesoporous structure with additional micropores.[15,16] The surfaces of the CDCs were functionalized by introducing oxygen-containing groups via heat treatment in air as well as reducing the oxygen content and minimizing the polarity of the surfaces by introducing chlorine surface functionalities via heat treatment in chlorine gas. Thereby, the influence of oxygen and halogen surface functionalities on the EDLC performance is examined for the $EMIBF_4$ IL electrolyte.

3.1. Material Characterization. Nitrogen physisorption (77 K) experiments were performed to characterize the porous structure of the pristine and surface-modified samples. The gas physisorption isotherms of all investigated samples (Figure 1a) show a distinct hysteresis loop, verifying the presence of a mesoporous structure. The resulting QSDFT PSDs are shown in Figure 1b and display a narrow size distribution of 4.1−4.2 nm for the mesopores of all investigated samples. The additional microporous structure of all OM-CDC samples, investigated in detail in our recent studies,[30] with a micropore volume (micro-PV) of 0.51−0.56 $cm^3\ g^{-1}$, is revealed (Table 1). Surface modifications of the pristine OM-CDC commonly maintain the SSA or PSD of the CDC samples.

The water-vapor adsorption measurements at 298 K show substantial influences of the different surface modifications on the surface polarities (Figure 2). The onset of water adsorption within the micropores is determined by the amount and strength of polar functional groups. This behavior is observed for the sample OM-CDC-air, which shows a distinct water adsorption at the lowest relative pressure of all investigated materials. Compared to pure OM-CDC, it contains more oxidic surface groups, leading to a polar carbon surface including acidic protons. In contrast, water adsorption occurs at higher relative pressures in chlorine-annealed OM-CDC, indicating the presence of a less polar surface in this material. As compared to the literature, the oxygen-containing surface groups are replaced by chlorine species of less polar character, hindering the water adsorption at low relative pressures.[31,32] The less polar surface of OM-CDC-Cl is also indicated by the lower total water uptake (1778 $cm^3\ g^{-1}$) compared to those of OM-CDC-air (2087 $cm^3\ g^{-1}$) and pristine OM-CDC (2069 $cm^3\ g^{-1}$), while similar total pore volumes are obtained from nitrogen physisorption measurements. The water adsorption in the OM-CDC pores at very high relative pressures is associated with the filling of the 4.1−4.2-nm-sized mesopores.

Table 1. Porosity of the OM-CDC Samples

sample	SSA[a] ($m^2\ g^{-1}$)	micro-PV[b] ($cm^3\ g^{-1}$)	TPV[c] ($cm^3\ g^{-1}$)	meso-PV[d] ($cm^3\ g^{-1}$)	mesopore size (nm)
OM-CDC	2838	0.56	2.03	1.47	4.2
OM-CDC-Cl	2901	0.56	2.03	1.47	4.1
OM-CDC-air	2765	0.51	1.98	1.47	4.1

[a]Multipoint BET surface area measured for P/P_0 = 0.05−0.2. [b]Cumulative micropore volume measured for pores <2 nm (QSDFT). [c]Total pore volume measured at P/P_0 = 0.95. [d]Mesopore volume calculated from meso-PV = TPV − micro-PV.

Raman experiments were performed to investigate the microstructure of the carbon samples (Figure 3). The spectra demonstrate similar degrees of graphitization and thus comparable microstructure and electrical conductivity for all investigated samples.

XPS was performed to quantify the surface heteroatoms (Figure 4). For OM-CDC-Cl, the amount of chlorine detected

dx.doi.org/10.1021/am4055029 | ACS Appl. Mater. Interfaces 2014, 6, 2922−2928

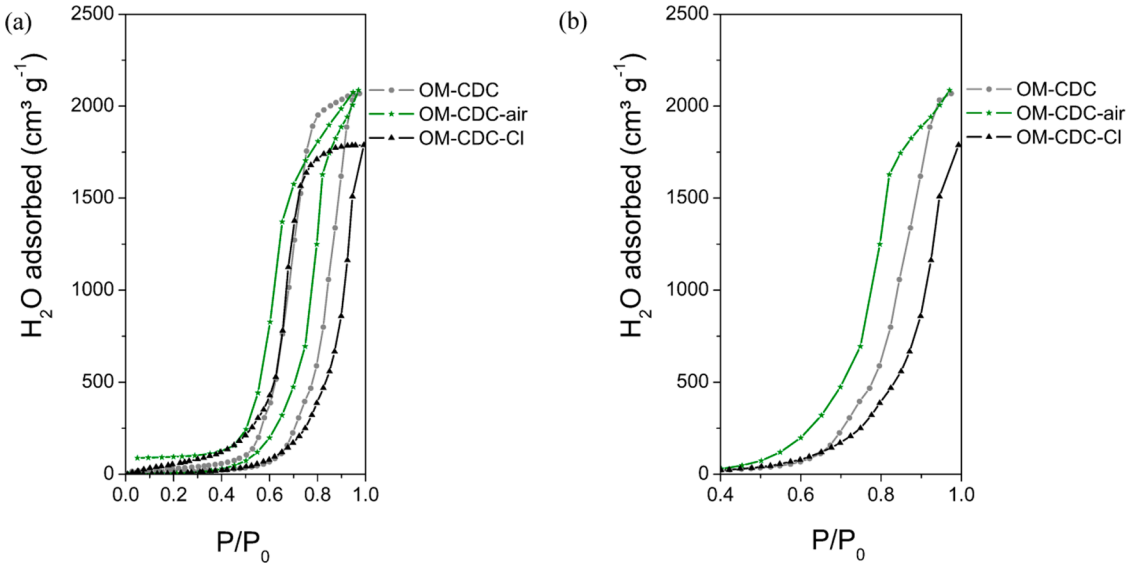

Figure 2. Surface analysis of OM-CDC samples: (a) Water-vapor adsorption and desorption isotherms recorded at 298 K. (b) Water adsorption branch: characteristics for the polarity of the microporous surface area of pristine and surface-modified OM-CDC samples.

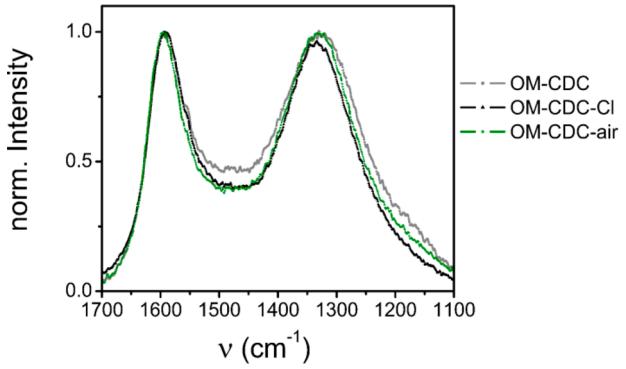

Figure 3. Raman spectra of pristine and surface-modified OM-CDC samples.

Table 2. Atomic Concentrations Calculated from High-Resolution XPS Spectra

sample	C (atom %)	O (atom %)	Cl (atom %)
OM-CDC	98.6	0.9	0.5
OM-CDC-Cl	96.2	1.0	2.8
OM-CDC-air	94.9	5.1	0

is increased in comparison to that for pristine OM-CDC (Figure 4c and Table 2).

This result provides additional proof for the successful surface halogenation of OM-CDC-Cl. In accordance with previous studies[31,32] and as was already verified by water-vapor adsorption measurements (Figure 2b), the surface polarity is decreased. The O 1s region of the XPS spectra clearly reveals the participation of oxygen heteroatoms located on the surface of the OM-CDC-air sample (Figure 4a), causing an increase in the surface polarity of the sample observed during water adsorption experiments (Figure 2b). For the air-exposed sample, the intensity shoulder at the high-energy side of the O 1s region points to a preferential increase of the amount of O−H bindings at the carbon surface.

As a consequence, only an insignificant variation of the SSA and pore structure is detected for pristine and surface-modified OM-CDCs. These materials merely differ in the surface polarity as well as content of oxygen surface functionalities and therefore in the presence and absence of acidic protons.[33] By tailoring the surface polarity as well as amount of acidic protons present on the carbon surfaces, we are able to systematically investigate their influence on the EDLC performance in IL electrolytes.

3.2. Electrochemical Investigations. In recent studies, an improved capacitive performance of surface-oxidized carbon compounds in aqueous electrolyte systems is caused by the increased wettability and pseudocapacitive reactions involving surface oxygen functionalities and accompanying acidic protons.[8,34−36] For organic solvent-based electrolytes, the wettability of carbon electrodes is affected by the hydrophilic

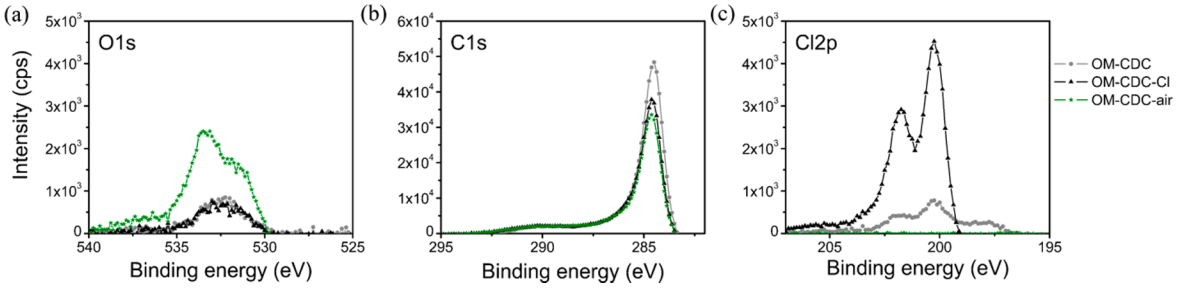

Figure 4. Surface analysis of pristine and surface-modified OM-CDC samples. XPS spectra of the (a) O 1s, (b) C 1s and (c) Cl 2p regions.

dx.doi.org/10.1021/am4055029 | ACS Appl. Mater. Interfaces 2014, 6, 2922−2928

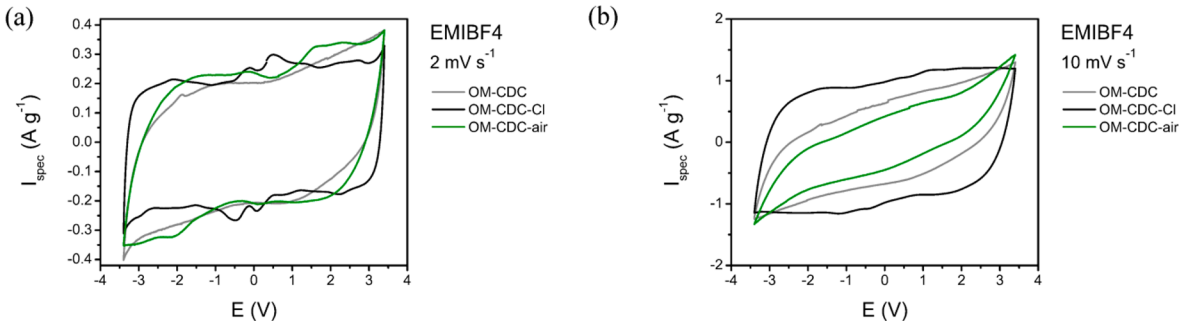

Figure 5. Electrochemical characterization of hexagonally ordered mesoporous carbon samples in $EMIBF_4$ IL at room temperature (298 K). Cyclic voltammogram measured at different scan rates of (a) 2 and (b) 10 mV s^{-1}.

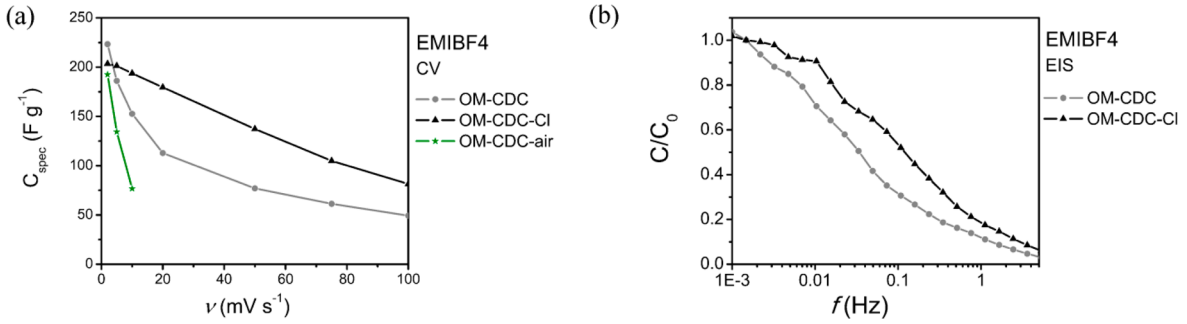

Figure 6. Electrochemical characterization of hexagonally ordered mesoporous carbon samples in $EMIBF_4$ IL at room temperature (298 K). (a) Specific capacitance (C_{spec}) of the OM-CDC samples calculated from the cyclic voltammogram measured at different scan rates. (b) PEIS experiments at open-circuit potential to test the rate capability. Capacitance calculated at a certain frequency (C) normalized to the capacitance calculated at f = 0.002 Hz (C_0) of the investigated sample.

or hydrophobic character determined by means of the polarity of the solvent.[37] For IL, on the contrary, the polarity does not correspond to the hydrophilicity and has to be discussed separately.[38] Lazzari et al.[18,21] and Jaramillio et al.[12] stated the negative effect of oxygen surface functionalities on the capacitive performance of mesoporous carbon compounds in hydrophobic IL electrolytes containing the TFSI anion. Jaramillo et al.[12] even hint at the possibility of increasing the capacitance performance by introducing halogen surface functionalities. Therefore, we investigated the electrochemical properties of our tailored surface-modified samples in combination with the $EMIBF_4$ IL electrolyte using CV at different scan rates (Figure 5) in a symmetric two-electrode cell setup. This setup is proven to provide the best evaluation of the electrode material's performance under real working conditions[39] to investigate the influence of the wettability and rate capability, on which our present study is addressed. To study additional redox processes taking place at the surface-modified samples, three-electrode measurements have to be performed. These will be the subject of further studies. The carbon samples tested in the $EMIBF_4$ IL electrolyte show a nearly rectangular CV shape at a low scan rate of 2 mV s^{-1} (Figure 5a), which is indicative of an EDLC performance even up to a voltage range of ±3.4 V and in accordance with previous studies in the literature.[40,41] All OM-CDC samples culminate at specific capacitances of 223 F g^{-1} (OM-CDC), 203 F g^{-1} (OM-CDC-Cl), and 238 F g^{-1} (OM-CDC-air) in the $EMIBF_4$ electrolyte. The difference in the EDLC performance in the IL electrolyte of pristine and surface-modified OM-CDC samples, however, becomes obvious in the shape of the CV curves as well as in the rate capability of the tested electrode materials (Figures 5 and 6). For pristine OM-CDC, distinct redox peaks are absent while the material is cycled in the wide potential range of ±3.4 V at a scan rate of 2 mV s^{-1}. For the surface-modified samples, however, additional redox peaks and thus changes in the interface formation behavior are revealed during charging and discharging. Because no redox peaks are observed for pristine OM-CDC, the latter peaks cannot be ascribed to electrolyte contaminations. Differences in the EDLC performance of OM-CDC-air and pristine OM-CDC are found by comparing their rate capabilities. OM-CDC-air shows a high capacitance decrease (60 %) compared to pristine OM-CDC (32 %) while the scan rate is increased from 2 to 10 mV s^{-1}. As reported by Palgunadi et al.,[41,42] this is attributed to the hydrogen-bond formation ability of the BF_4^- anions of the electrolyte. The anions might be attached to the surface functionalities, hindering their movement along the surface of the narrow micropores of the OM-CDC-air sample and blocking these pores for the reversible electrostatic charge accumulation at high polarization rates (high scan rates). The strong drop of the capacitance for OM-CDC-air in hydrophilic $EMIBF_4$ underlines the insufficient description of the occurring effects by the hydrophilic/hydrophobic physical property concept of IL electrolytes at carbon/IL interfaces. The improved rate capability of pristine OM-CDC is attributed to its less polar surface as well as the smaller amount of surface acidic protons due to the lower content of surface oxygen groups, as proven by water-vapor adsorption experiments and XPS. This trend is further supported by the additional improvement of the rate capability (5% capacitance decrease while raising the scan rate from 2 to 10 mV s^{-1}) observed for the surface-treated OM-CDC-Cl sample. Surface halogenation decreases the polarity of the carbon surfaces[31,32] and leads to a thermal destabilization of the oxygen groups. Thus, this

dx.doi.org/10.1021/am4055029 | ACS Appl. Mater. Interfaces 2014, 6, 2922−2928

treatment is an opportunity to remove the latter groups from the carbon surface while simultaneously protecting it against reoxidation.[43]

Therefore, for the first time, surface halogenation was systematically proven to improve the power density because of the better rate performance of porous carbon electrodes while testing for supercapacitor application using the $EMIBF_4$ IL electrolyte. A drastically improved rate capability was verified for the workable symmetrical two-electrode setup, revealing a 27% increased specific capacitance determined for the chlorine-treated OM-CDC at a scan rate of 10 mV s^{-1}, contrary to a 50% decrease observed for oxygen-treated OM-CDC, all compared to the pristine material.

Further investigations including potentiostatic electrochemical impedance spectroscopy (PEIS) at the open-circuit potential were carried out to evaluate the supercapacitor performance. The impedance spectroscopy experiments applied a potential oscillation to the symmetric two-electrode supercapacitor test cell. The resistance behavior of the cell is predominant at high oscillation frequencies, whereas at low oscillation frequencies, the capacitance behavior becomes predominant. The transition area in the mid-frequency range is governed by the migration rates of the electrolyte ions (e.g., determined by the porosity of the electrode material) and interactions between the electrode and electrolyte.[44] By evaluation of the low- and mid-frequency range from f = 0.002 to 7.9 Hz, the specific capacitance of the electrode material is calculated according to eq 2

$$C_{spec} = \frac{2}{2\pi f \,\mathrm{Im}(Z)\, m} \tag{2}$$

where C_{spec} is the specific capacitance (F g^{-1}) based on the mass m of the electroactive material of a single electrode, f is the operating frequency (Hz), and Im(Z) is the imaginary part of the measured impedance (Ω). When the capacitance at a certain frequency (C) is normalized to the maximum capacitance calculated at f = 0.002 Hz (C_0) of the investigated sample, the differences in the rate capabilities of OM-CDC and OM-CDC-Cl become even more obvious (Figure 6b). Pristine OM-CDC tends to an early capacitance drop at frequencies <0.02 Hz. By surface halogenation of the OM-CDC-Cl sample, the rate capability is represented by a distinct plateau of up to frequencies >0.02 Hz. The results of the OM-CDC-air sample are spared because the PEIS mid-frequency experiments are mostly dominated by a resistive behavior unable to be analyzed for capacitance calculations, according to eq 2.

4. CONCLUSIONS

Hexagonally OM-CDC was modified in surface chemistry to improve the overall capacitive performance of supercapacitors, utilizing IL $EMIBF_4$ as the electrolyte. Our studies reveal the influence of surface functional groups on the capacitance performance. The surface treatment of pristine OM-CDC in chlorine gas protects the surface from reoxidation and lowers the surface polarity, thus enhancing the rate capability, which results in an, at least, 27% higher specific capacitance of the pristine porous electrode material at scan rates greater than or equal to 10 mV s^{-1}. The surface treatment of OM-CDC in air introduces oxygen functionalities, which results in a significant decrease of the rate capability. This decrease in the power density is caused by an increase in the surface polarity and the incidence of acidic protons as part of the oxygen functionalities, causing a drastic decrease of at least 50% in specific capacitance at a scan rate greater than or equal to 10 mV s^{-1} compared to the pristine material. Future simulation studies of the porous carbon/IL interfaces should therefore include various surface functionalities to disclose more precise information about their influence on the EDLC performance on an atomistic or quantum-chemical scale.

AUTHOR INFORMATION

Corresponding Author

*Tel: +49 351 4659 690. E-mail: k.pinkert@ifw-dresden.de.

Author Contributions

The manuscript was written through contributions of all authors. All authors have given approval to the final version of the manuscript.

Notes

The authors declare no competing financial interest.

ACKNOWLEDGMENTS

The authors thank S. Hampel for providing the Raman spectrometer and F. Budig for executing the electrochemical measurements. This work has been financed by the European Union (ERDF) and the Free State of Saxony (SAB) in the framework of the European Centre for Emerging Materials and Processes (ECEMP) under Grant 100111670.

REFERENCES

(1) Simon, P.; Gogotsi, Y. *Nat. Mater.* **2008**, *7*, 845−854.
(2) Goodenough, J. B.; Park, K.-S. *J. Am. Chem. Soc.* **2013**, *135*, 1167−1176.
(3) Rolison, D. R.; Nazar, L. F. *MRS Bull.* **2011**, *36*, 486−493.
(4) Aricò, A. S.; Bruce, P. G.; Scrosati, B.; Tarascon, J.-M.; van Schalkwijk, W. *Nat. Mater.* **2005**, *4*, 366−377.
(5) Bruce, P. G.; Freunberger, S.; Hardwick, L. J.; Tarascon, J. M. *Nat. Mater.* **2011**, *11*, 19−30.
(6) Sillars, F. B.; Fletcher, S. I.; Mirzaeian, M.; Hall, P. J. *Phys. Chem. Chem. Phys.* **2012**, *14*, 6094−6100.
(7) Bose, S.; Kuila, T.; Mishra, A. K.; Rajasekar, R.; Kim, N. H.; Lee, J. H. *J. Mater. Chem.* **2012**, *22*, 767−784.
(8) Hao, L.; Li, X.; Zhi, L. *Adv. Mater.* **2013**, *25*, 3899−3904.
(9) Xiao, N.; Tan, H.; Zhu, J.; Tan, L.; Rui, X.; Dong, X.; Yan, Q. *ACS Appl. Mater. Interfaces* **2013**, *5*, 9656−9662.
(10) Brandt, A.; Balducci, A. *J. Electrochem. Soc.* **2012**, *159*, A2053−A2059.
(11) Brandt, A.; Pohlmann, S.; Varzi, A.; Balducci, A.; Passerini, S. *MRS Bull.* **2013**, *38*, 554−559.
(12) Jaramillo, M. M.; Mendoza, A.; Vaquero, S.; Anderson, M.; Palma, J.; Marcilla, R. *RSC Adv.* **2012**, *2*, 8439−8446.
(13) Rose, M.; Korenblit, Y.; Kockrick, E.; Borchardt, L.; Oschatz, M.; Kaskel, S.; Yushin, G. *Small* **2011**, *7*, 1108−1117.
(14) Korenblit, Y.; Rose, M.; Kockrick, E.; Borchardt, L.; Kvit, A.; Kaskel, S.; Yushin, G. *ACS Nano* **2010**, *4*, 1337−1344.
(15) Krawiec, P.; Kockrick, E.; Borchardt, L.; Geiger, D.; Corma, A.; Kaskel, S. *J. Phys. Chem. C* **2009**, *113*, 7755−7761.
(16) Borchardt, L.; Oschatz, M.; Lohe, M.; Presser, V.; Gogotsi, Y.; Kaskel, S. *Carbon* **2012**, *50*, 3987−3994.
(17) Balducci, A.; Dugas, R.; Taberna, P. L.; Simon, P.; Plee, D.; Mastragostino, M.; Passerini, S. *J. Power Sources* **2007**, *165*, 922−927.
(18) Lazzari, M.; Soavi, F.; Mastragostino, M. *Fuel Cells* **2010**, *10*, 840−847.
(19) Armand, M.; Endres, F.; MacFarlane, D. R.; Ohno, H.; Scrosati, B. *Nat. Mater.* **2009**, *8*, 621−629.
(20) Kurig, H.; Vestli, M.; Tonurist, K.; Janes, A.; Lust, E. *J. Electrochem. Soc.* **2012**, *159*, A944−A951.
(21) Lazzari, M.; Mastragostino, M.; Soavi, F. *Electrochem. Commun.* **2007**, *9*, 1567−1572.

(22) Kondrat, S.; Pérez, C. R.; Presser, V.; Gogotsi, Y.; Kornyshev, A. *Energy Environ. Sci.* **2012**, *5*, 6474−6479.
(23) Borchardt, L.; Oschatz, M.; Paasch, S.; Kaskel, S.; Brunner, E. *Phys. Chem. Chem. Phys.* **2013**, *15*, 15177−15184.
(24) Largeot, C.; Taberna, P. L.; Gogotsi, Y.; Simon, P. *Electrochem. Solid-State Lett.* **2011**, *14*, A174−A176.
(25) Vatamanu, J.; Hu, Z.; Bedrov, D.; Perez, C.; Gogotsi, Y. *J. Phys. Chem. Lett.* **2013**, *4*, 2829−2837.
(26) Lazzari, M.; Soavi, F.; Mastragostino, M. *J. Electrochem. Soc.* **2009**, *156*, A661−A666.
(27) Lazzari, M.; Mastragostino, M.; Pandolfo, A. G.; Ruiz, V.; Soavi, F. *J. Electrochem. Soc.* **2011**, *158*, A22−A25.
(28) Sun, W.; Jiang, Q.; Wang, Y.; Jiao, K. *Sens. Actuators, B* **2009**, *136*, 419−4124.
(29) Moulder, J. F.; Stickle, W. F.; Sobol, P. E.; Bomben, K. D. *Handbook of X-ray Photoelectron Spectroscopy*; Chastain, J., King, R. C., Jr., Eds.; Physical Electronics, Inc.: Eden Prairie, MN, 1995.
(30) Oschatz, M.; Borchardt, L.; Rico-Francés, S.; Rodríguez-Reinoso, F.; Kaskel, S.; Silvestre-Albero, J. *Langmuir* **2013**, *29*, 8133−8139.
(31) MacDonald, J. A. F.; Evans, M. J. B.; Liang, S.; Meech, S. E.; Norman, P. R.; Pears, L. *Carbon* **2000**, *38*, 1825−1830.
(32) Hall, C. R.; Holmes, R. J. *Carbon* **1992**, *30*, 173−176.
(33) Bandosz, T. J.; Buczek, B.; Grzybek, T.; Jagiello, J. *Fuel* **1997**, *76*, 1409−1416.
(34) Lufrano, F.; Staiti, P. *Int. J. Electrochem. Sci.* **2010**, *5*, 903−916.
(35) Liu, X.; Zhou, L.; Zhao, Y.; Bian, L.; Feng, X.; Pu, Q. *ACS Appl. Mater. Interfaces* **2013**, *5*, 10280−10287.
(36) Wang, R.; Wang, P.; Yan, X.; Lang, J.; Peng, C.; Xue, Q. *ACS Appl. Mater. Interfaces* **2012**, *4*, 5800−5806.
(37) Kühnel, R.-S.; Obeidi, S.; Lübke, M.; Lex-Balducci, A.; Balducci, A. *J. Appl. Electrochem.* **2013**, *43*, 697−704.
(38) Stoller, M. D.; Ruoff, R. S. *Energy Environ. Sci.* **2010**, *3*, 1294−1301.
(39) Weingarth, D.; Foelske-Schmitz, A.; Kötz, R. *J. Power Sources* **2013**, *225*, 84−88.
(40) Weingarth, D.; Noh, H.; Foelske-Schmitz, A.; Wokaun, A.; Kötz, R. *Electrochim. Acta* **2013**, *103*, 119−124.
(41) Palgunadi, J.; Hong, S. Y.; Lee, J. K.; Lee, H.; Lee, S. D.; Cheong, M.; Kim, H. S. *J. Phys. Chem. B* **2011**, *115*, 1067−1074.
(42) Perez-Cadenas, A. F.; Maldonado-Hodar, F. J.; Moreno-Castilla, C. *Carbon* **2003**, *41*, 473−478.
(43) Kurig, H.; Jänes, A.; Lust, E. *J. Electrochem. Soc.* **2010**, *157*, A272−A279.
(44) Taberna, P. L.; Simon, P.; Fauvarque, J. F. *J. Electrochem. Soc.* **2003**, *150*, A292−A300.